

Chapter 5

Influence of grain size and anisotropic viscosity on the development of an anisotropic layer in the upper mantle

Abstract

The degree of anisotropic viscosity and the grain size of upper mantle minerals are two important rheological parameters that are generally poorly constrained. We use numerical models of asthenospheric flow to determine the grain size and anisotropic viscosity required to explain the observed confinement of seismic anisotropy to a layer at the top of the convecting upper mantle. We find that a grain size larger than 10 mm gives the best fit to the observations. The ratio of shear viscosity to normal viscosity is 0.3 or more, depending on grain size.

5.1 Introduction

Seismic anisotropy is the direction-dependence of seismic wave speeds. In the upper mantle below the oceans, radial seismic anisotropy appears to be confined within a layer extending from the base of the lithosphere to a depth of about 200 km (Dziewonski and Anderson, 1981; Gung et al., 2003; Smith et al., 2004; Beghein et al., 2006). The maximum anisotropy under the oceans is observed at a depth of about 120 km (Debayle et al., 2005; Nettles and Dziewonski, 2008), which is approximately 45 km below the 'Gutenberg discontinuity',

sometimes identified as the base of the lithosphere (Revenaugh and Jordan, 1991). If plate motion relative to the lower mantle is shearing the entire upper mantle, one would expect the anisotropy to extend further down, perhaps as far down as the olivine-spinel phase transition. The observation that the anisotropy is, instead, confined to the topmost part of the convecting mantle seems to require special conditions. We propose that a grain-size dependent and anisotropic composite rheology play an important role.

Strain in the mantle partitions among various microscopic deformation mechanisms by which mantle rocks deform. Laboratory studies on the deformation of olivine point to two main deformation mechanisms in action in the Earth’s upper mantle: diffusion creep and dislocation creep (see Drury and FitzGerlad (2000) for a review). Diffusion creep (also known as Cobble creep) takes place by the diffusion of atoms and vacancies primarily along grain boundaries. Diffusion creep is also sometimes referred to as “grain-size sensitive” creep, due to the strong dependence of the viscosity on grain size ($\eta \propto d^3$). Dislocation creep involves slip along a finite number of crystallographic glide planes and directions. “Power-law creep” is an alternative name for dislocation creep, emphasizing the strong dependence of the strain rate on the applied stress ($\dot{\epsilon} \propto \sigma^{3.5}$). The development of lattice preferred orientation (LPO) is usually considered to require deformation by dislocation creep (e.g. Karato et al., 1995; Fliervoet and Drury, 1999; Warren and Hirth, 2006).

Preferred orientation leads to anisotropy not only of seismic wave speeds but also of material strength. Anisotropic viscosity has been shown to change flow in a range of mantle dynamics scenarios, from thermal convection (Richter and Daly, 1978; Moresi et al., 2003), Rayleigh-Taylor instabilities (Lev and Hager, 2008a) to continental break-up (Vauchez et al., 1997). Still, the strength of mechanical anisotropy in the mantle is poorly constrained. Using laboratory experiments, Durham and Goetze (1977) showed that the strain rate of creeping olivine with preexisting fabric depends on the orientation of the sample and can vary by up to a factor of 50. This is because the orientation of the sample relative to the applied stress determines which slip systems are activated. In the experiments of Bai and Kohlstedt (1992) on high-temperature creep of olivine, and those of Wendt et al. (1998) on peridotites, the measured strain rate depended strongly on the relative orientation of the applied stress to

the sample crystallographic axis. The effect of shape-preferred orientations on the strength in a deformed two-phase composite material has not yet been studied experimentally, and theoretical estimations rely on simple geometrical assumptions (Weijermars, 1992; Mandal et al., 2000; Treagus, 2003).

The characteristic grain size in the upper mantle is also poorly constrained, despite the strong dependence of the rheology on it. Samples from lithospheric xenoliths and ophiolites show a fractal distribution of grain sizes, with most grains smaller than 5mm but a substantial number between 5 and 20mm. Based on modeling of dehydration and grain size evolution, Eisenbeck (2009) and Behn et al. (2009) predict that the grain size in the oceanic upper mantle at a depth of 150km should be ~ 11 mm. Our goal in this paper is to constrain grain size and anisotropy using seismic observations and flow models.

5.2 Methods

We construct two-dimensional models of simple shear – approximating the flow beneath a moving rigid plate and a sluggish mantle at depth. We vary the plate velocity, the grain size and the degree of anisotropic viscosity assumed for the mantle material. We then calculate the depth and the width of the shear zone that develops at the base of the plate, as well as the depth and width of the region which deforms dominantly by dislocation creep.

5.2.1 Model setup

Our model domain is a two-dimensional box extending 900 km horizontally and 300 km vertically. The depth of the box represents the part of the upper mantle extending from the base of the lithosphere at a depth of 80 km down to 380 km, just above the transition of olivine to the spinel mineral phase.

We use a composite rheology to account for the combination of the dislocation creep and the diffusion creep deformation mechanisms. The effective viscosity of the composite is defined by its two constituents:

$$\frac{1}{\eta_{effective}} = \frac{1}{\eta_{diffusion}} + \frac{1}{\eta_{dislocation}} \quad (A0)$$

The viscosities of the two components are calculated using the constitutive equation and material constants reported by Hirth and Kohlstedt (2003) for olivine with a constant water content:

$$\eta = \left[A^{-1} d^p f H_2O^{-r} \exp\left(\frac{E^* + PV^*}{RT}\right) \right]^{1/n} \times (2\dot{\epsilon})^{\frac{1-n}{n}} \quad (A0)$$

where the $\dot{\epsilon}$ is the strain rate, R is the gas constant, T is the absolute temperature and P is the pressure. The parameters we use are listed in table 5.1.

Definition	Symbol	Units	Diffusion creep value	Dislocation creep value
Pre-exponent constant	A	–	10^6	90
grain size	d	μ m	varied	varied
grain size exponent	p	–	3	0
water content	$f H_2O$	$H/10^6 Si$	1000	1000
water content exponent	r	–	1	1.2
activation energy	E^*	J/mol	335000	480000
activation volume	V^*	$10^{-6} m^3/mol$	4	11
stress exponent	n	–	1	3.5

Table 5.1: Values of constants used in viscosity calculation

Both the temperature and pressure are assumed to be solely a function of the depth z , where $P(z) = \rho g z$ and $T(z)$ is calculated as:

$$T(z) = T_0 + \frac{\Delta T}{\Delta z} z \quad (A0)$$

The geothermal gradient $\frac{\Delta T}{\Delta z}$ is taken as $0.3 \text{ } ^\circ/km$ (Turcotte and Schubert, 2002). The resulting upper mantle viscosity profiles are plotted in Figure 5-1.

The dislocation creep component is allowed to develop anisotropic viscosity in order to model the mechanical anisotropy of rocks with strong lattice preferred orientations. We explore a range of values for the ratio between the shear and normal viscosities $\eta_s/\eta_N \equiv \delta$,

using $\delta \in \{0.1, 0.25, 0.5, 0.75, 1\}$, with $\delta = 1$ representing isotropic viscosity. This range of ratios is supported by lab experiments (Durham and Goetze, 1977; Bai and Kohlstedt, 1992) and field observations (Warren et al., 2008). The preferred orientation develops as described in chapter 6 (Lev and Hager, 2008b). The grain sizes in the models are $d \in \{1, 2, 5, 7.5, 10, 20\}mm$.

For the calculations shown here, we apply a constant velocity boundary condition of 80 mm/yr to the bottom of the box. The top surface is held fixed. The sides are free to move horizontally but not vertically. Material can leave and enter the box through the side walls. It is important to note here that the selected plate velocity has very little effect on the results. This is a direct outcome from the constitutive laws defining dislocation and diffusion creep used here. The partitioning of strain between the two components is controlled by the non-dimensional ratio of the viscosities. Let us write the constitutive laws for the isotropic case ($\delta = 1$) as:

$$\eta^{diff} = \eta_0^{diff} \times \left(\frac{d}{d_0}\right)^p \quad \text{and} \quad \eta^{disl} = \eta_0^{disl} \times \left(\frac{\dot{\epsilon}_0}{\dot{\epsilon}}\right)^{\frac{n-1}{n}}$$

where η_0 are reference viscosities, d_0 a reference grain size and $\dot{\epsilon}_0$ a reference strain rate. For $p = 3$, $n = 3.5$, the viscosity ratio is proportional to $\frac{d^3}{\dot{\epsilon}^{0.7}}$, which implies that a change of an order of magnitude in the imposed velocity or strain rate is equivalent to a change of the grain size by only a factor of 1.6.

5.2.2 Numerical tools

We solve the equations of flow, expressing the conservation of mass and momentum, using the finite-element method as implemented in the public-domain software package *Underworld* (Moresi et al., 2007). *Underworld* combines an Eulerian grid-based finite-element formulation with a particle-based Lagrangian integration point scheme. The material points in *Underworld* are used for tracking tracking material properties, in particular material orientation and anisotropy. The rectangular finite-elements in our grid all have a uniform size of 10 by 5 km.

To account for the anisotropic viscosity we use a simplified constitutive law that assumes a transversely isotropic (TI) material. This kind of anisotropy can be characterized by two

viscosities – a shear viscosity η_s and a normal viscosity η_N (Honda, 1986). Mühlhaus et al. (2002b) define the following constitutive law using the orientation tensor Λ_{ijkl} :

$$\sigma_{ij} = -p\delta_{ij} + 2\eta_N\dot{\epsilon}_{ij} - 2(\eta_N - \eta_S)\Lambda_{ijkl}\dot{\epsilon}_{kl} \quad (\text{A0})$$

where σ is the stress tensor, $\dot{\epsilon}$ is the strain rate tensor. The orientation of the TI material enters the constitutive law through the orientation tensor Λ . It is calculated by tracking of a large set of directors, oriented particles representing the normals to the easy glide planes of the TI material (Mühlhaus et al., 2002b). We use 60 directors for each of the ≈ 5400 finite-element cells, for a total of over 300,000 directors. To better represent the recrystallization that accompanies the development of lattice preferred orientation, we include the forced realignment technique described by Lev and Hager (2008a).

5.2.3 Analysis of flow models output

After a calculation reaches a steady state we calculate two values: the “strata with sufficient strain” (SWiSS) and the expected delay time from teleseismic shear-wave splitting. Combined, these parameters indicate where we can expect an anisotropic layer in the mantle.

Strata with sufficient strain (SWiSS)

We define the “strata with sufficient strain” as the region which, after the entire model has accumulated 70% engineering shear strain, has itself accumulated at least 70% strain. We use this cut-off value following the results of Zhang et al. (2000), who demonstrated alignment of olivine LPO with the shear direction experiments after 70% engineering shear strain. A finite shear strain of 0.7 occurs when the displacement across a layer is equal to the thickness of the layer. Given a velocity profile as a function of depth, $v(z)$, the relative displacement across a layer of thickness Δz after a time t is $t\frac{\partial v}{\partial z}\Delta z$. We can therefore define a criteria for sufficient straining of a layer: $t\frac{\partial v}{\partial z}\Delta z > \Delta z$. The time to accumulate 70% engineering shear strain across the entire model is $t = Z_0/V_p$, where Z_0 is the box depth and V_p is the plate velocity. In our simple shear model, $\frac{\partial v}{\partial z} = \dot{\epsilon}$. We can define a normalized strain rate $\dot{\epsilon}^* = \dot{\epsilon}/V_p$ and

obtain the following criteria for sufficient shear strain: $\varepsilon^* > 1/Z_0$.

SKS splitting times

To obtain a proxy of how the anisotropy obtained in our models would appear in seismic observations, To estimate the time delay that a split teleseismic shear wave will experience as it travels vertically through the model domain, we first need to calculate how much of the model material can develop a lattice preferred orientation. It is widely assumed that the development of LPO requires deformation by dislocation creep, and thus we need to examine the way in which strain rate in our model is partitioned between the two deformation mechanisms we considered – diffusion creep and dislocation creep. We calculate the viscosities of the two components ($\eta_{diffusion}$ and $\eta_{dislocation}$) and then assume that the strain rate fraction is inversely proportional to the relative viscosity of each component:

$$F_{dislocation} = \eta_{diffusion} / (\eta_{diffusion} + \eta_{dislocation}) \quad (A0)$$

SKS split time: Once we find the fraction of dislocation creep deformation as a function of depth, we convolve it with the SWiSS, and calculate the accumulated split time as follows:

$$dV_s(z) = \begin{cases} 0 & z \notin SWiSS \\ 0.25 \times F_{dislocation}(z) & z \in SWiSS. \end{cases} \quad (A0)$$

which uses a 0.25 km/s difference between the fast and slow phases by taking $V_{slow} = 4.58$ km/s and $V_{fast} = 4.75$ km/s (Savage, 1999). We also assume a linear relationship between the partitioning of diffusion and dislocation creep, the strength of the LPO and the resulting seismic anisotropy. The accumulated delay time is:

$$dt = \int_{bottom}^{top} \left(\frac{1}{V_0 - dV_s(z)} - \frac{1}{V_0 + dV_s(z)} \right) dz \quad (A0)$$

where V_0 is the average shear wave velocity.

5.3 Results

Depth profiles of the strain rate for models with a grain size of $d = 10\text{mm}$ and a range of δ values are shown in Figure 5-2. The figure also shows the cut-off value defining the SWiSS. The profiles demonstrate the relationship between anisotropic viscosity and localization of strain into a narrow zone.

The depth extent of the SWiSS as a function of the grain size d and the viscosity ratio δ is plotted in the contour map in Figure 5-3. The SKS splitting times are shown in Figure 5-4. Both plots reveal that a value of $\delta = 0.5$ for a grain size of 10mm, and $\delta > 0.3$ for grains larger than 15mm, are capable of reproducing the depth extent of the anisotropic layer in the upper mantle as observed by Debayle et al. (2005) and Nettles and Dziewonski (2008). a viscosity ration of 0.1 leads to a highly localized shear zone (only 10 km wide) at the top of the model domain. Such a narrow zone of aligned anisotropic material would result in mechanical decoupling of the lithosphere and the asthenosphere. It seems however that such localization is inconsistent with the seismic observations.

5.4 Discussion

As we mentioned earlier, constraints from seismic observations place most of the anisotropy in the upper mantle beneath the oceans to within a layer that reaches 200 km, with the maximal anisotropy observed at 120km depth (Debayle et al., 2005; Nettles and Dziewonski, 2008). The combination of parameters that gives us the best fit to this depth is $\delta = 0.3$ and d greater than 10mm. This result gives us a lower bound on anisotropic viscosity in the upper mantle, an important rheological parameter which is poorly constrained.

Our conclusion relies on the observations of seismic anisotropy. The observation of a strongly anisotropic layer beneath the oceans with a maximum anisotropy at 120km depth is shared by many studies, and appears to be robust (see a discussion by Kustowski et al. (2008)). We must keep in mind, though, that most of the constraints on the depth extent of anisotropy in the upper mantle come from the analysis of surface waves, and specifically of the difference in velocities of Rayleigh and Love waves. The depth region in which most of the

anisotropy is found is sometimes considered a problematic region for surface wave analysis, as the sensitivities of Love waves diminishes rapidly with depth at this exact range, while the sensitivity of Rayleigh waves extends deeper (e.g. Nettles and Dziewonski, 2008, Figure 1). These differences might be mapped to anisotropy, leading to overestimation of the depth extent of the anisotropy. If the depth of upper mantle anisotropy is indeed overestimated, the constraint we can place on δ and d would no longer be as tight. However, the results of studies using different techniques, for example normal modes (Beghein et al., 2006), do not differ significantly from those of studies using surface waves.

We find that the grains need to be larger than 10mm to explain the observed layer of seismic anisotropy in the upper mantle. Mercier and Nicolas (1975) suggest a grain size of 10mm for the xenoliths collected in the Alps and in Hawaii. A similar value is reported by Armienti and Tarquini (2002). Samples from ophiolites usually come from shallower depths in the mantle, closer to the Moho, but they too exhibit maximum grain sizes of 8-12mm (e.g. Dijkstra et al., 2002).

From the viscosities and strain rates in our model we can estimate the stress: taking mantle viscosity to be $10^{18}Pas$ (see Figure 5-1) and the strain rates to be on the order of $10^{-14}1/sec$ (Figure 5-2), the stress is about 0.01MPa. Using the data of Karato (1980), plotting $d = 80\mu m$ against $\sigma = 100MPa$, a stress of 0.01MPa is in equilibrium with a grain size of over 1m (using the piezometer of Hall and Parmentier (2003), scaling $d \propto \sigma^{-n/p} = \sigma^{-1.17}$) or 0.8mm (using the paleowattmeter formulation of Austin and Evans (2007), scaling $d \propto \sigma^{-1/(1+p)} = \sigma^{-0.25}$). Our estimated grain size falls within this wide range, and is closer to the latter value, which uses an algorithm considered to be more robust (Behn et al., 2009). Eisenbeck (2009) and Behn et al. (2009) also find that grains at depth of 150km in the oceanic upper mantle should be $\sim 11mm$ large.

Some caution must be taken when using the experimentally-derived constitutive laws and constant to interpret the results of our models. There is a trade-off between uncertainty in the constant coefficients A in equation 5.2.1 for both diffusion creep and dislocation creep, and uncertainty in the calculated grain size. What is important in our kinematic models is the ratio of these two constants. Experimental uncertainty in the A ratio is estimated

to be a factor of 2. If A is in fact twice as small as the value we use, this translates to a change of 30% in the grain size. Since we predict grains that are larger than 10 mm, the uncertainty in grain size due to uncertainty in A is about 3 mm. In addition, the published values of the activation volumes V^* for olivine range between 0 to $30 \text{ cm}^3/\text{mol}$ (Korenaga and Karato, 2008), with the activation volume of dislocation creep the least constrained value. If the V_{disl}^* is much higher (> 20 instead of $4 \text{ cm}^3/\text{mol}$), the zone in which deformation is accommodated by dislocation creep will be limited to shallow depth, unless the grains are much larger ($d > 20\text{mm}$). However, the overall viscosity profile for the upper mantle would then reach values on the order of 10^{22} Pas , considerably higher than accepted estimates (e.g. Hager, 1991). Changing the geothermal gradient to $0.5^\circ/\text{km}$ moves the depth of $\eta_{diffusion} = \eta_{dislocation}$ about 40 km shallower, but the composite viscosity profile and the relative viscosities of the two components at the at the uppermost part do not change much. We therefore believe that our results are not very sensitive to the selection of the geothermal gradient.

5.5 Conclusion

By successfully reproducing the observed confinement of seismic anisotropy to a 50km thick layer beneath the oceanic lithosphere, we are able to place a lower bound on the grain size and constrain the degree of anisotropic viscosity in the upper mantle. We find that anisotropic viscosity should be 0.5 for a grain size of 10mm. For larger grains ($d > 15$), the viscosity ratio can be between 0.3 and 1.

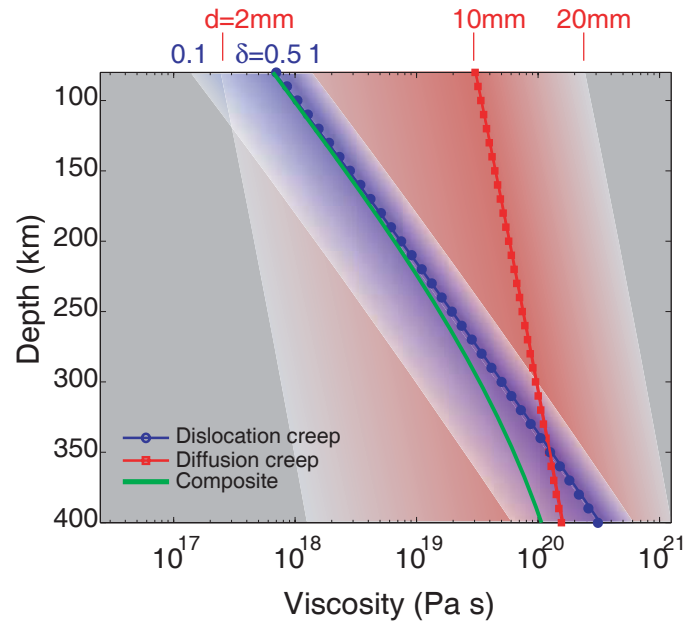


Figure 5-1: Depth profiles of the viscosity of the diffusion creep component (red), dislocation creep component (blue) and the composite material (green). The red shaded area shows the variation of diffusion creep viscosity for grain sizes ranging from 2 to 20mm. The blue shaded area shows the variation of dislocation creep viscosity multiplied by a range of δ values from 0.1 to 1.

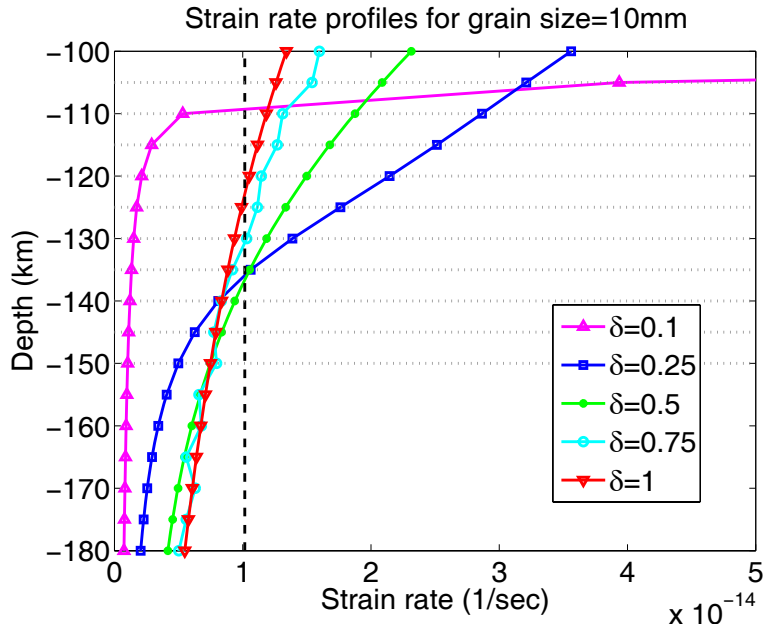


Figure 5-2: Strain rate profiles with depth for models with grain size $d = 10\text{mm}$. The vertical dashed line shows the cut-off criteria defining the zone with sufficient strain. The curves reveal the correlation between δ and the thickness of the zone of localized strain.

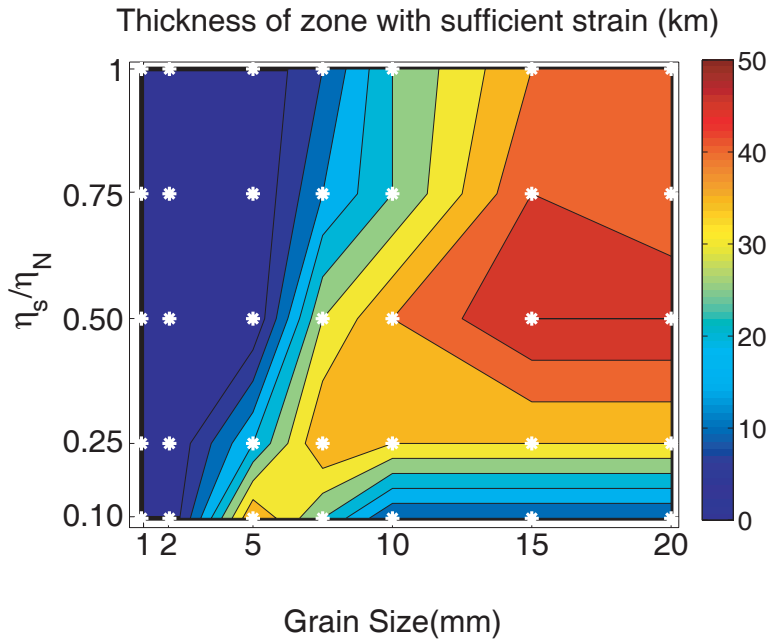


Figure 5-3: Thickness of the zone with sufficient as a function of the the grain size d and viscosity contrast δ . Areas in warm colors indicate thicknesses of 40 km or more, which are consistent with seismic observations. Cool colors indicate parameter values that give a layer that is either too thin (mostly for to low δ values) or that the strain rate is not high enough (grains too small).

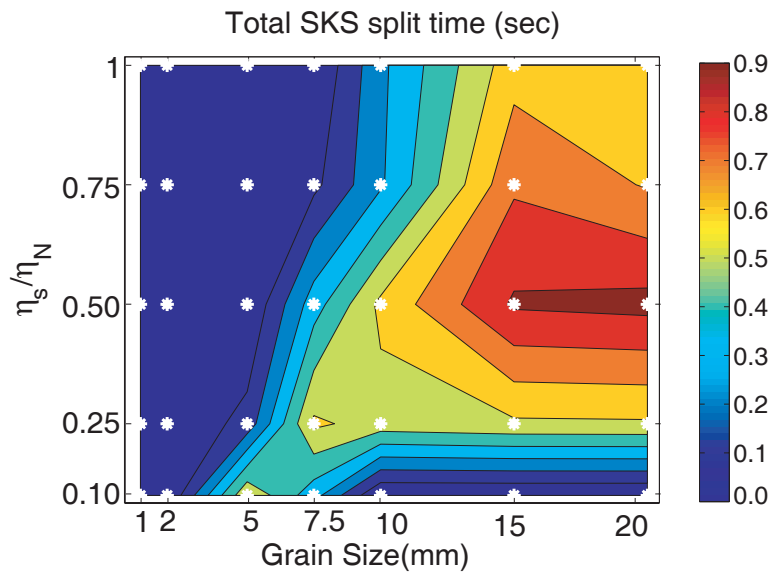


Figure 5-4: SKS delay times as a function of the the grain size d and viscosity contrast δ .

